EXPERIMENTAL INVESTIGATION OF INTERFACIAL FRACTURE PARAMETERS AND CRACK INITIATION UNDER MECHANICAL AND THERMOMECHANICAL LOADING

P. Ganeshan, H. V. Tippur, J. K. Sinha

EXPERIMENTAL INVESTIGATION OF INTERFACIAL FRACTURE PARAMETERS AND CRACK INITIATION UNDER MECHANICAL AND THERMOMECHANICAL LOADING

P. Ganeshan
H. V. Tippur
J. K. Sinha
Department of Mechanical Engineering
Auburn University
Auburn University, Alabama, USA

Mechanically and thermomechanically stressed interface cracks in adhesively bonded bimaterials (PMMA-aluminum) with a large elastic and thermal property mismatch are experimentally studied. The elasto-optic effects are mapped as $(\sigma_x + \sigma_y)$ contours in the PMAA halves and interfacial fracture parameters are estimated. Crack initiation under mechanical and thermomechanical loading conditions are shown to be controlled by different micromechanical processes. The results suggest that the micromechanical unlocking of microcavities and microprotrusions along the interface is primarily responsible for failure initiation under thermomechanical loading conditions. This is unlike the mechanical loading situations wherein fracture toughness is derived primarily from the breakage of interlocking microentanglements. The measured values of the fracture parameter $\Delta Im(Ka^{i\varepsilon})_T$ due to a temperature rise is a constant and much higher than its real counterpart $(\Delta\psi_T(a) \approx 76 - 82°)$. The $(\Delta(Ka^{i\varepsilon})_T|_{cr}$ thus obtained are much lower than the mechanical counterparts.

Adhesively bonded bimaterial systems are used in many engineering applications. In these, interfaces tend to be the planes of weakness due to the presence of disbonds. Owing to the mechanical and thermal properties mismatch, interfacial defects often experience severe stresses during service. In recent years a number of bimaterial fracture mechanics investigations specifically dealing with interface cracks subjected to mechanical loading have been reported. It is generally observed that cracks or disbonds laying along interfaces undergo mixed-mode deformations owing to the elastic properties mismatch. Hence, fracture toughness of interfaces depend on mode-mixity, which in turn depends on the elastic mismatch. Williams [1] first demonstrated the characteristic oscillatory singularity of bimaterial interface cracks. Rice and Sih [2] developed explicit relations for two-dimensional near tip stress fields. Several studies [3–9] reported since address specific issues pertaining to (i) modeling crack tip deformations and characterizing crack tip fields using complex stress intensity factors and (ii) developing testing methods and fracture

specimens to evaluate interface fracture toughness as a function of mode-mixity. Hutchinson and Suo [10] and Rice [11] reviewed the progress of interfacial fracture mechanics in recent years.

The fracture parameters and the failure mechanisms when interfaces are subjected to combined thermal and mechanical loads depend both on thermal and elastic properties mismatch as well as the nature of the bond, namely, mechanical interlocking, diffusion, adsorption, and chemical, for example. Owing to the complexity of the problem, relatively fewer studies can be found on this topic. The effect of thermal load on interface crack was investigated analytically by Brown and Erdogan [12] and more recently by Kuo [13]. Finite element analysis is carried out by Kokini [14] to study the effect of transient thermal load in ceramic-metal bimaterials. Kokini and Smith [15] studied the effects of bond thickness and heat flux direction on the interfacial crack tip fields using photoelasticity. Interfacial crack growth in thermomechanically loaded bimaterial joints were examined numerically by Hermann et al. [16].

In this article, optical measurement of stresses and fracture parameters for cracks lying along interfaces in mechanically and thermomechanically stressed bimaterial systems is reported. Relative characteristics of stress fields and failure mechanisms are studied in these two situations. Of primary interest are failure of interfaces, which derived strength from micromechanical interlocking. Edge-bonded interfacial systems consisting of PMMA-aluminum sheets are studied. The bimaterial system offers a large stiffness mismatch as well as a large thermal properties mismatch across the interface. First, a full-field optical method, *Mach-Zehnder interferometry* (MZI), is developed for studying local stress fields near interface cracks. The method offers high-sensitivity and real-time stress measurement capabilities. MZI is first used to measure interfacial crack tip stresses in three-point bend specimens, and critical values of fracture parameters are assessed. Subsequently, transient thermal stresses induced by heating the aluminum halves of three-point bend specimens are mapped using MZI. Estimates of *stress intensity factors* (SIFs) are obtained by analyzing the interference patterns. The fracture parameters and fracture surface are examined to identify the differences in the crack initiation mechanisms in mechanical and thermomechanical situations.

MACH-ZEHNDER INTERFEROMETRY

In this section, the working principle and the physical interpretation of interference patterns of a MZI are discussed. The optical setup is shown schematically in Figure 1. The light source is a 10-mW He-Ne laser beam expanded and collimated to a 50-mm diameter. The interferometer consists of a reference optical path 1 and a test optical path 2 created using two beam splitters (BS1, BS2) and two mirrors (M1, M2). The two beams are recombined after M2, and the interference patterns are recorded using a camera. An optically isotropic transparent fracture specimen is placed in the test path 2. When 50/50 beam splitters are used, the complex
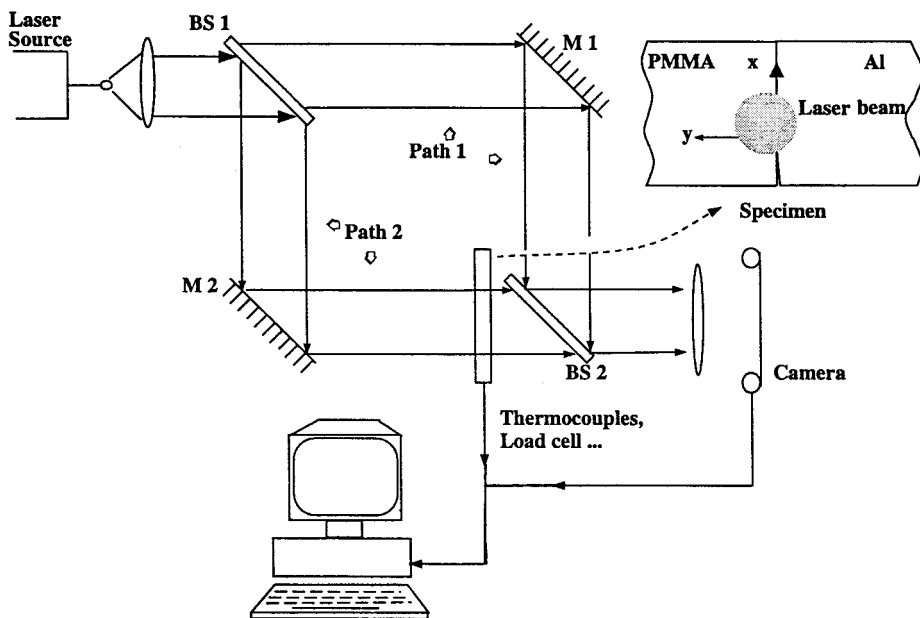
Figure 1. Schematic of Mach–Zehnder interferometer and experimental setup.

spatial amplitude distribution, E_1, and E_2, corresponding to paths 1 and 2, are

$$E_1 = A_0 \exp(ikl)$$
$$E_2 = A_0 \exp(ik[l + \Delta l + (n_0 - 1)B]) \tag{1}$$

where l represents the nominal geometric length of the two paths, Δl represents a constant difference in lengths between the two paths that might result during the alignment of the interferometer, k $(= 2\pi/\lambda)$ is the wave number, and n_0 and B are the refractive index and the nominal thickness of the test specimen, respectively. Hence, the intensity distribution on the camera plane corresponding to the undeformed specimen is

$$I = 2A_0^2(1 + \cos k[\Delta l + (n_0 - 1)B]) \tag{2}$$

For constructive interference on the image plane,

$$k[\Delta l + (n_0 - 1)B] = 2N\pi$$
$$\text{or} \quad \Delta l + (n_0 - 1)B = N\lambda \tag{3}$$

where N is the fringe order ($N = 0, \pm 1, \pm 2, \ldots,$). Since Δl, n_0, and B are constants, N represents a uniform "infinite" fringe corresponding to the initial planarity of the object wavefront.

When the specimen undergoes deformation under isothermal conditions, E_2 changes to

$$E_2 = A_0 \exp\left(ik\left[l + \Delta l + (n_0 - 1)B + \delta S^{EO}(x, y)\right]\right) \tag{4}$$

where $\delta S^{EO}(x, y)$ is the optical path change in the specimen due to a combination of the stress-optic effect and the Poisson effect and is a function of in-plane spatial coordinates (x, y) of the specimen

$$\delta S^{EO}(x, y) = 2 B(n_0 - 1)\int_0^{1/2} \varepsilon_z \, d(z/B) + 2B\int_0^{1/2} \delta n_0 \, d(z/B) \tag{5}$$

The first term in Eq. (5) represents the net optical path difference due to the plate thickness change $(\varepsilon_z = (1/E)(\sigma_z - \nu(\sigma_x + \sigma_y)))$ or Poisson effect. The second term is due to a stress-induced refractive index change $(= \text{Constant} \times (\sigma_x + \sigma_y + \sigma_z))$ or the stress-optic effect in the material. Hence, the intensity distribution for the deformed specimen is given by

$$I = 2 A_0^2\left(1 + \cos k\left[\Delta l + (n_0 - 1)B + \delta S^{EO}(x, y)\right]\right) \tag{6}$$

Again, for constructive interference,

$$k\left[\Delta l + (n_0 - 1)B + \delta S^{EO}\right] = 2 N'\pi$$
$$\text{or} \quad \delta S = (N' - N)\lambda = \mathcal{N}\lambda \tag{7}$$

where $\mathcal{N}'$, $\mathcal{N} = (N' - N) = 0, \pm 1, \pm 2, \ldots$. From the preceding analysis it is clear that interference patterns represent contours of constant $\delta S^{EO}(x, y)$ and the sensitivity of measurement is equal to λ per fringe. When mechanical loads are applied to the transparent object, a combination of stress-optic effect and Poisson effect constitute δS^{EO} as in Eq. (5). The path difference can be related to the mechanical field [5] using plane stress assumptions ($\sigma_z = 0$) as follows:

$$\delta S^{EO} = cB(\sigma_x + \sigma_y) = \mathcal{N}\lambda \tag{8}$$

where c is the elasto-optic constant for the material. The value of c for PMMA is -0.92×10^{-10} m^2/N [17].

It should be noted that the thermo-optical effects (δS^{TO}) could also contribute to the optical path difference. That is, changes in the refractive index and the thickness of the object due to temperature changes (ΔT) could contribute to the optical field. In the presence of such changes, the optical path difference can be expressed as

$$\delta S^{total} = \delta S^{EO} + \delta S^{TO} = \mathcal{N}\lambda \tag{9}$$

in which, $\delta S^{TO} = (\delta S^{RI} + \delta S^B)$, where δS^{RI} $(= (d(n_0 - 1)/dT)(\Delta T)B)$ and δS^B $(= (n_0 - 1)\alpha(\Delta T)B$, where α is the coefficient of thermal expansion of the phase object) are the optical path length changes due to temperature-induced refractive index and thickness changes, respectively.

INTERFACIAL CRACK TIP FIELDS AND MEASUREMENT OF FRACTURE PARAMETERS

Mechanically Stressed Bimaterial

Bimaterial specimens were made by bonding equal thickness sheets ($B = 6$ mm) of PMMA and aluminum (see Figure 2(a)). Special care was exercised while matching PMMA to avoid machining stresses. The PMMA was machined using a high-speed
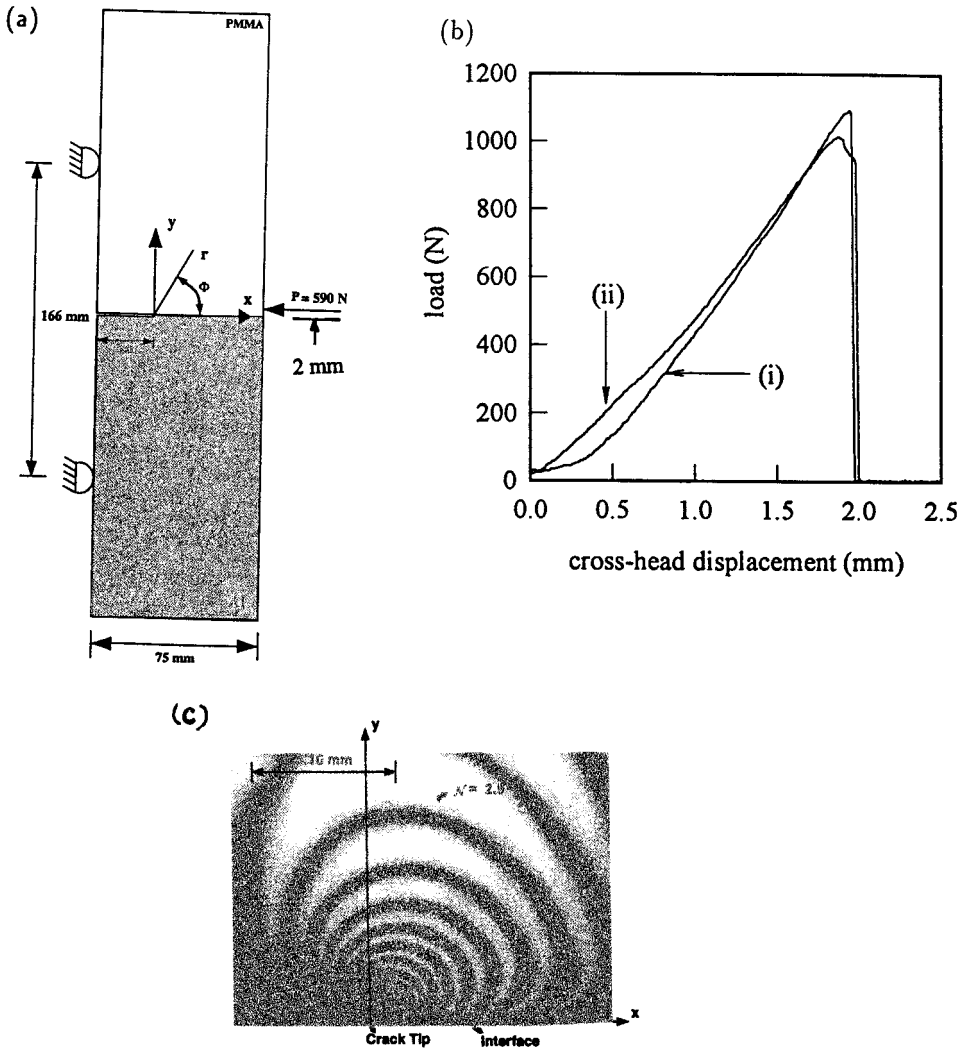

Figure 2. (a) Bimaterial specimen and (b) typical load vs. displacement plots for bimaterial beams (i) with and (ii) without a Teflon tape insert. Surface roughness $R_a \approx 4.5$ μm. (c) Crack tip fringes of $cB(\sigma_x + \sigma_y)$ in the PMMA half under mechanical loading.

milling (950 rpm) during which chilled water mist was used as a coolant. A small depth of cut (250 μm per run) and 125 mm/min feed rate was maintained during the process. The aluminum half of the specimen was machined and sand blasted (roughness $R_a \approx 4.5$ μm) prior to bonding to promote micromechanical interlocking, which results in good bond strength. The bonding procedure consisted of in situ polymerization of *methylmethacrylate* (MMA) monomer at room temperature. An edge crack along the interface ($a/W = 0.33$) was introduced using soft, pliable Teflon tape (thickness < 50 μm) during the bonding procedure. The two halves of the bimaterial were held together during the curing period by applying uniform pressure on the interface. The applied pressure helped squeeze the Teflon tape to produce a crack with a much smaller root radius. The Teflon tape used to introduce the discontinuity in the bimaterials specimens ensured consistent production of straight crack fronts. It should be noted that the use of debonding agents produced the so-called "zero-thickness" crack but ensuring a straight crack front was difficult. The failure response of three-point bend specimens with and without the Teflon tape inserts are shown in Figure 2(*b*). Evidently, the failure loads (peak loads) are nearly the same in both the cases.

The samples were loaded in a displacement controlled loading (cross-head speed ≈ 2 mm/min) device. The load cell output and marker signals from a motorized 35-mm camera were acquired using a data acquisition system. The marker signal from the camera provided a one-to-one correspondence between the load levels and the individual frames registered on the film strip. The event was started by an external trigger and interference patterns were imaged at a framing rate of 20 frames/min. A typical fringe pattern in the PMMA portion of the beam is shown in Figure 2(*c*) for an applied load $P = 590$N. The ($\sigma_x + \sigma_y$) increment between two successive dark (or light) fringes is approximately 1.1 MPa.

Considering the preceding material the interface ($0 < \phi < \pi$) and following Rice [11], the asymptotic expression for MZI fringes can be derived as

$$cB(\sigma_x + \sigma_y) = e^{\varepsilon(\phi - \pi)} r^{-1/2} [\, A_1 \cos(-\phi/2 - \varepsilon \ln(r/a))\,]$$

$$+ e^{\varepsilon(\phi - \pi)} r^{-1/2} [\, B_1 \sin(-\phi/2 - \varepsilon \ln(r/a))\,]$$

$$+ r^0 [\, A_2\,]$$

$$+ e^{\varepsilon(\phi - \pi)} r^{1/2} [\, A_3 \cos(\phi/2 - \varepsilon \ln(r/a))\,]$$

$$+ e^{\varepsilon(\phi - \pi)} r^{1/2} [\, B_3 \sin(\phi/2 - \varepsilon \ln(r/a))\,]$$

$$+ r^1 [\, A_4 \cos(\phi)\,]$$

$$+ r^1 [\, B_4 \sin(\phi)\,] + \cdots$$

$$= N\lambda \qquad N = 0, \pm 1, \pm 2, \ldots \qquad (10)$$

where A_n and B_n $(n = 1, 2, 3, \ldots)$ are the constant coefficients of the asymptotic expansion, $A_1 + iB_1$ is proportional to the complex stress intensity factor $(Ka^{i\varepsilon})$

$$A_1 + iB_1 = \frac{2\,cB}{\sqrt{2\pi}\,\cosh(\pi\varepsilon)}(Ka^{i\varepsilon})$$

ε is the oscillation index

$$\varepsilon = \frac{1}{2\pi}\ln\frac{\mu_1 + \mu_2\,\kappa_1}{\mu_2 + \mu_1\,\kappa_2}$$

μ_α is the shear modulus, and $\kappa_\alpha = (3 - \nu_\alpha)/(1 + \nu_\alpha)$ $(\alpha = 1$: PMMA; $\alpha = 2$: aluminum) for plane stress. For a PMMA-aluminum interface $\varepsilon = 0.098$. The crack tip mode-mixity (or phase angle of $(Ka^{i\varepsilon})$) ψ and energy release rate G are defined as

$$\psi(a) = \tan^{-1}\left[\operatorname{Im}(Ka^{i\varepsilon})/\operatorname{Re}(Ka^{i\varepsilon})\right] \tag{11}$$

$$G = \frac{1}{E'}\frac{K\overline{K}}{\cosh^2(\pi\varepsilon)} \qquad \frac{1}{E'} = \frac{1}{2}\left(\frac{1}{E_1} + \frac{1}{E_2}\right) \tag{12}$$

where E_α denotes Young's modulus. When nonsingular higher order contributions are negligible compared to the singular term (first two terms in Eq. (10)), it reduces to the so-called K-dominant form.

The images were digitized around the crack tip along discrete radial directions to collect fringe location (r, ϕ) and fringe order $(\mathcal{N})$ data. An overdeterministic least squares routine was used for optical information processing and only the data beyond $(r/B) = 0.5$ and between $45°$ and $135°$, where the deformations are shown to be predominantly two dimensional [8, 9], were used to estimate the crack tip parameters. Generally, the exact number of terms required to account for the nonsingular contributions to the crack tip field is unknown a priori. Therefore, higher order terms (in Eq. (10)) were included sequentially to improve the agreement between the measured data and least squares fit and simultaneously achieve numerical convergence of the estimated values of stress intensity factors. The parameter estimation procedure consisted of minimizing the error function $\Phi(r, \phi; A_1, B_1, A_2, A_3, B_3, \ldots)$ $(= \Sigma_{i=1}^{m}[F_i - F_i^{\exp}]^2;$ F and $F^{\exp}$ are the right-hand sides in Eq. (10), m denotes the total number of data points) with respect to the constants of the series A_n and B_n $(n = 1, 2, 3, \ldots)$. Details of the procedure are reported elsewhere [8, 9]. A sample result from the fringe analysis corresponding to two terms (unknown coefficients A_1, B_1) and five terms (unknown coefficients A_1, B_1, A_2, A_3, B_3) are shown in Figures 3(a, b), respectively. When only K-dominant terms in Eq. (10) were used in the analysis, the synthetic fringes (solid lines) and the digitized data (symbols) do not agree well with each other. Furthermore, the measured value of $(Ka^{i\varepsilon} = (0.89 + i0.19)$ MPa$\sqrt{\mathrm{m}}$) do not match well with the computed value [6] of $(Ka^{i\varepsilon}) = (1.33 + i0.17)$ MPa$\sqrt{\mathrm{m}}$. When the nonsingular terms
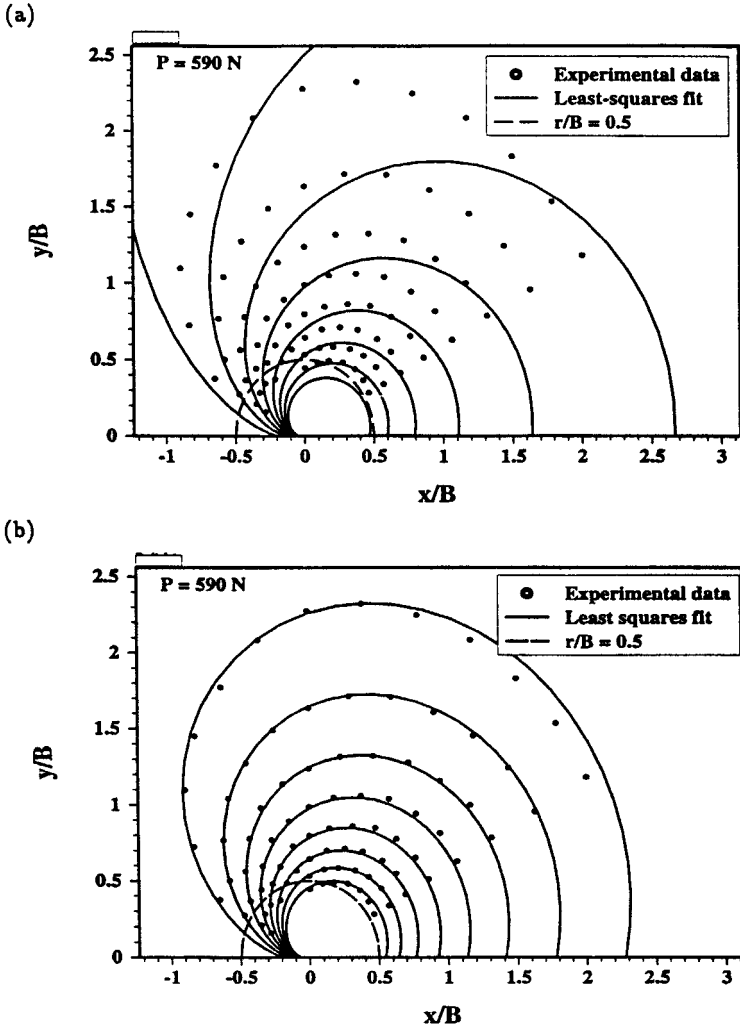
(a)

(b)

Figure 3. Least squares analysis to extract interfacial fracture parameters for the case of mechanical loading. Analysis for (*a*) two terms and (*b*) five terms. Data within the semicircle ($r/B = 0.5$) are not used in the analysis.

were considered in the analysis, the match between the data and the synthetic curves was significantly improved and the measured fracture parameter was ($Ka^{i\varepsilon}) = (1.33 + i0.25)$), which agrees well with the numerical values. Note that in Figures 3(*a*, *b*), the semicircle indicates the $r/B = 0.5$ boundary and the data points shown within this semicircle were blocked during the analysis; the entire data set is shown for completeness.

The applied load P was increased monotonically and the load at crack initiation was noted as P_{cr-m}. Subsequently, the energy release rate at crack

initiation G_{cr} was calculated. Based on four repeatable tests, in which P was applied at a small distance (2 mm) away from the interface, $P_{cr-m} \approx 925N$ and hence the energy release rate ($\propto P^2$) $G_{cr-m} \approx 610$ J/m^2 (or $|K_{cr}| \approx 2.1$ Mpa$\sqrt{m}$) at a mode-mixity $\psi(a) \approx 10.5°$ (or $\hat{\psi}(\hat{a}=0.001$ m$) \approx -10°$) were determined. These values fall within the range of crack initiation toughness values previously reported [8, 18] for the same bimaterial system. Note that the measured value of $|K_{cr}|$ is somewhat higher than the value for homogeneous PMMA ($K_{Ic} = 1.8$ MPa$\sqrt{m}$) subjected to mode-I loading [19]. However, since the interfacial crack tip deformation is inherently mixed-mode in nature, the presence of shear (particularly negative shear) ($\hat{\psi}(\hat{a}=0.001$ m$) = -10°$) on the interfacial plane is known generally to enhance the crack initiation toughness ($|K_{cr}|$) values [18].

Thermo Mechanically Stressed Bimaterial

The bimaterial fracture specimens used for mapping thermally induced crack tip stresses have the same dimensions as those used for mechanical loading tests. The components of the bimaterial system have a large thermal property mismatch. The ratio of coefficients of thermal expansion for PMMA and aluminum is $\alpha_1:\alpha_2 \approx$ 3.3:1. (Also, the thermal conductivity ratio is $k_1:k_2 \approx 1:8.5$; thus PMMA is essentially a thermal insulator compared to aluminum.) Three-point bending specimens were subjected to different initial loads (P) and then heated. Two thermofoils (75 mm$\times$ 75 mm) were attached to the faces of the aluminum halves away from the interface for heating the specimen. The nominal resistance of each of the resistors connected in parallel was 14Ω and the supply voltage was 45V. The rate of heating was controlled by the input voltage using a variac, and temperatures at different locations across the interface and near the crack tip were measured using T-type thermocouples. Also, during the experiments the exposed surfaces of the aluminum half of the specimen were kept thermally insulated. Note that the initial load applied to the specimen kept the crack "open" during the experiments. Moreover, for a positive oscillation index ε and heat flux from material-2 to material-1, a small far-field tensile stress is necessary for maintaining the validity of a "small-scale contact" assumption [13]. The influence of the magnitude of the initial load is discussed later in this section.

MZI was used to map interference patterns proportional to ($\sigma_x + \sigma_y$) near the crack and along the interface. The region of examination was a semicircle of 50-mm diameter near the interfacial crack tip in the PMMA half of the specimen. The samples were first subjected to an initial load. The thermomechanical experiments were then started by an external trigger than initiated a data acquisition system, voltage supply to the heating elements, and the camera. During the event, the voltage outputs from the load cell, the thermocouples, and the camera were all acquired simultaneously. The interference patterns were imaged at a framing rate of 20 frames/min. Typical fringe patterns at two different times are shown in Figures 4(a, b) for the case of an initial applied load of $P/P_{cr-m} \approx 0.25$. It is important to note the large material properties mismatch between the two materi-
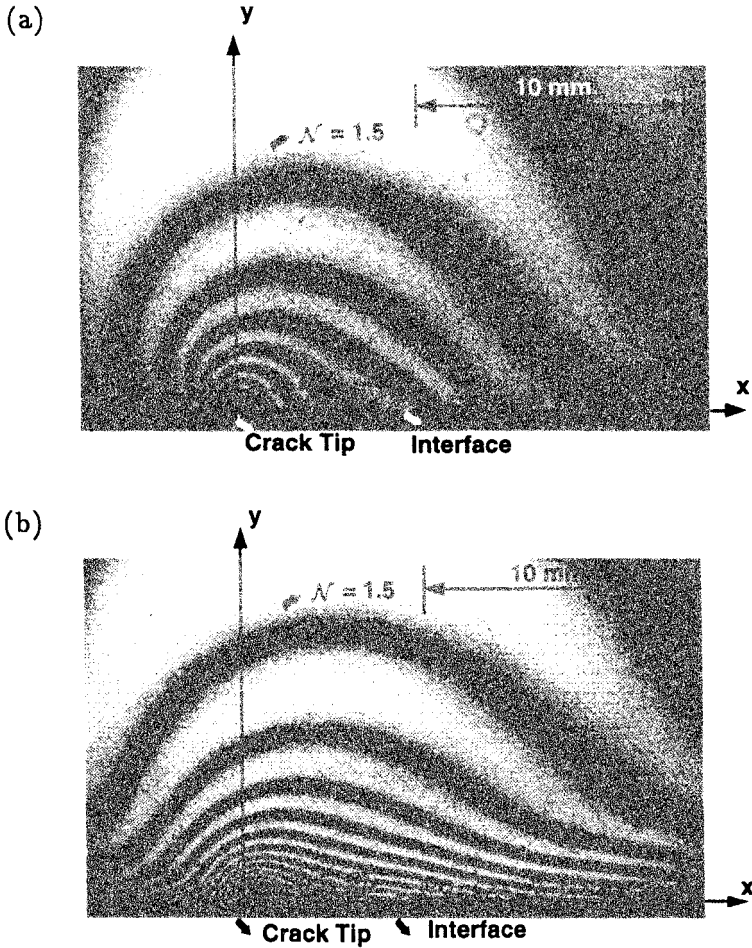
(a)

(b)

Figure 4. Interfacial crack tip contours of $cB(\sigma_x + \sigma_y)$ in the PMMA half of the specimen when the specimen is subjected to thermal-mechanical loading: (*a*) $t = 36$ sec and (*b*) $t = 54$ sec.

als and PMMA as being a rather poor conductor of heat; the deformations occur in PMMA without any significant rise in the temperature in PMMA. The influence of the thermal field on fringes will be discussed later in this section. The thermocouple data acquired until crack initiation during the experiment is shown in Figure 5. The measured data indicates a rapid but similar increase in temperature at points A, B, and C on the aluminum side of the interface. Note that the temperature in aluminum increases to about $70°$ C, which is substantially lower than the glass-transition temperature $T_g \approx 110°$C for PMMA. During the same time interval, measured temperatures at three locations (D, E, F) and on the PMMA side of the specimen indicate a rather small temperature increase. At a distance of 3 mm $(r/B = 0.5)$ the temperature rise is only about $5°$C.
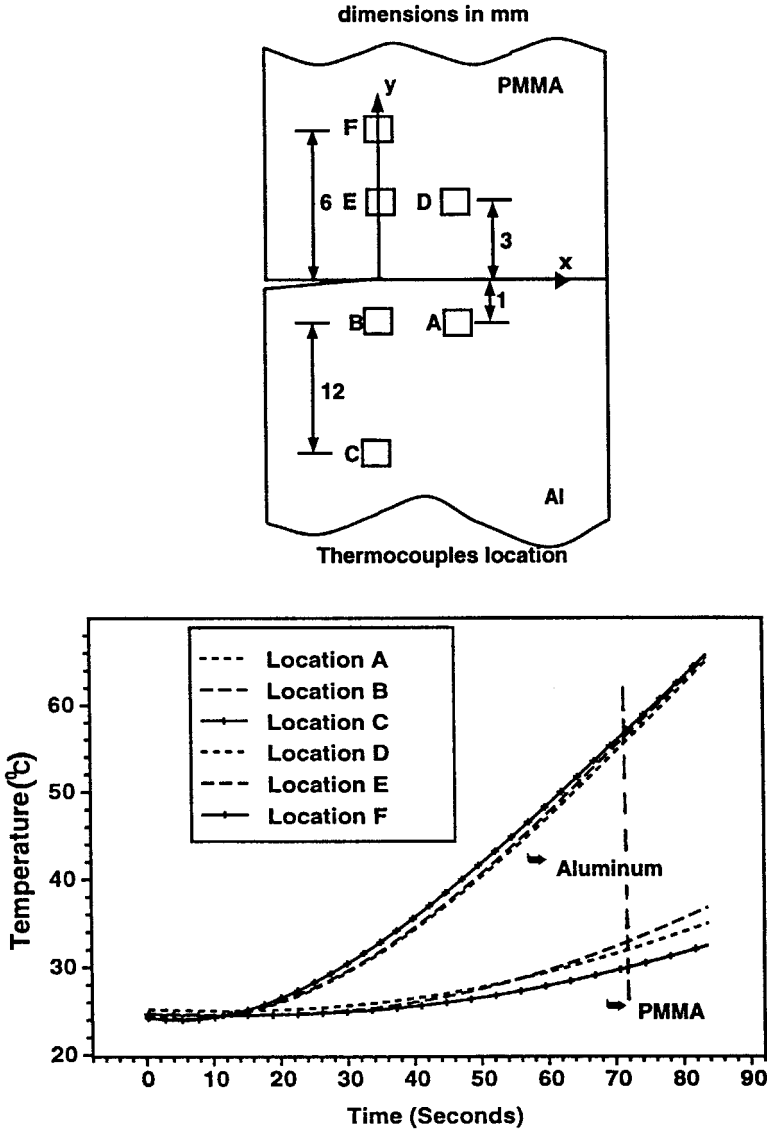
Figure 5. Measured temperature data in the vicinity of the interfacial crack and the interface.

To estimate the influence of the temperature rise on the fringes (δS^{TO} in Eq. (9)), an experiment with *unbonded* (*and unconstrained*) bimaterial beam was carried out. The rate of change of refractive index with temperature (dn_0/dT) for PMMA is reported [20] to be of the order of $-10^{-5}/°$C and the coefficient of thermal expansion values range between $7.6-8.3\times 10^{-5}/°$C. Hence, this experiment also helped deal with such variations in the thermal properties reported for

PMMA. The two halves of a mechanically fractured bimaterial were held together using elastic bands and heated as in bonded bimaterials described earlier. The interference fringes in the interfacial region at $t = 0$ and $t = 70$ sec and the temperature at point E are shown in Figures 6(a–c). Evidently, the temperature rise at point E (Figure 6(c)) is nearly identical to that shown in Figure 5; hence it could be concluded that an intimate contact between the two halves existed during the experiment. More importantly, a relatively small number of fringes (about three fringes in Figure 6(b)) are formed along the interface during this period in a region within the half-plate thickness distance. This suggests that the thermo-optic effects are relatively small compared to the elasto-optical effects. The primary reason for this is the refraction index, and thickness changes have opposite signs and produce self-compensating effect to a large extent. Furthermore, the optical data for extracting stress intensity factors come from regions beyond the half-plate
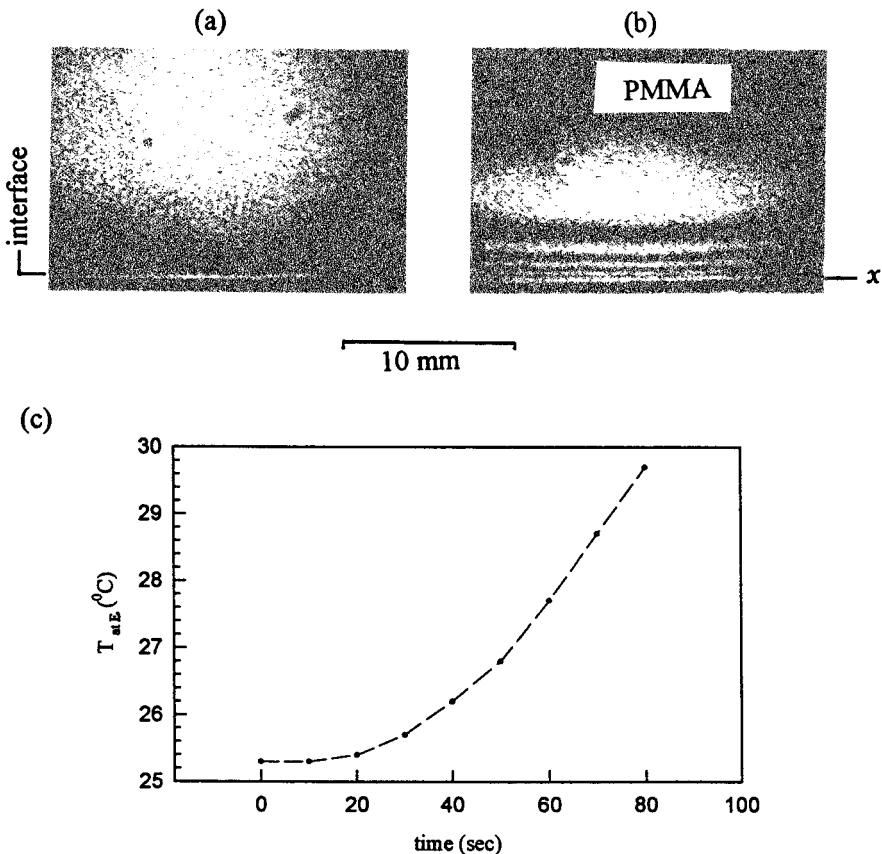

Figure 6. Influence of thermo-optical effects: interference patterns at (a) $t = 0$ sec and (b) $t = 70$ sec and (c) temperature rise at point E.

thickness distance from the crack tip and the interface and hence an analysis based on elasto-optical effect is sufficient in these cases.

It is evident from Figure 4 that when the temperature rises in the aluminum half of the specimen, the mismatch in thermal properties introduce additional stresses along the interface and near the crack tip. The temperature rise introduces a large relative thermal expansion along the interface, causing an increase in the crack tip shear deformations. It also introduces a small increase in the load P to $P + \Delta P_\mathrm{T}$, where ΔP_T is the temperature-induced incremental load due to three-point constraint. Parallel fringes clustered along the interface indicate large stress gradients perpendicular to the interface and all along the crack tip and represent dominant interfacial shear effects. One method of extracting interfacial fracture parameters from these interference patterns is to use the asymptotic expansion field (Eq. (10)) since no additional singularities are introduced by the imposed thermal field [13, 21]. In doing so, however, numerical difficulties due to ill-conditioned matrices were encountered in the least squares analysis due to a large number of higher order terms (compared to the mechanical counterpart) needed to fit the optical data satisfactory. A modified approach of using higher order terms that are specific to a given problem along with K-dominant terms is shown to alleviate this problem [22]. That is, the optical field is viewed as a superposition of a K-dominant field and the experimentally determined higher order terms specific to the problem on hand. One can determine the nature of the higher order terms necessary for analyzing the interface patterns by examining the fringe order variation across the interface far from the crack tip in an unconstrained bimaterial specimen. Figure 7 shows fringes across the interface in an *unconstrained bimaterial specimen* subjected to heating in the same way three-point bend specimens were heated. It is evident from the interference pattern away from the crack tip that fringes are essentially parallel to the interface and a plot of fringe order $\mathcal{N}$ vs. nondimensional distance y/B suggests a quadratic higher order term of the type $C_1 + C_2 y + C_3 (y)^2$, where the C_is are unknown constants. Thus, by superposing the K-dominant field and the observed higher order terms we have

$$cB(\sigma_x + \sigma_y) \approx e^{\varepsilon(\phi - \pi)} r^{-1/2} [A_1 \cos(-\phi/2 - \varepsilon \ln(r/a))]$$

$$+ e^{\varepsilon(\phi - \pi)} r^{-1/2} [B_1 \sin(-\phi/2 - \varepsilon \ln(r/a))]$$

$$+ C_1 + C_2 y + C_3 y^2$$

$$= \mathcal{N}\lambda \qquad \mathcal{N} = 0, \pm 1, \pm 2, \ldots \qquad (13)$$

where A_1 and B_1 are related to the complex SIF as before. An overdeterministic least squares analysis with basis functions on the right-hand side of Eq. (13) was used to analyze the digitized fringes obtained from thermal-mechanical tests. Again, the data in regions potentially affected by crack tip and interface three-dimensionality were excluded from the analysis. Results from a least squares
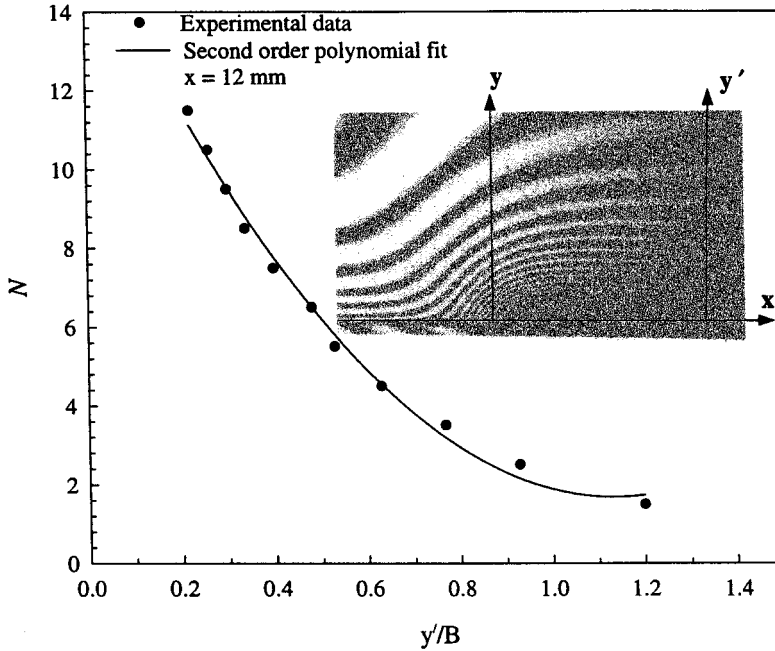
Figure 7. Interference fringes and Fringe order variation across the interface along y' away from the interface crack tip.

analysis for two instances of time are shown in Figure 8 and good agreement between the fringe data and the fit are evident outside the semicircular region of radius $r/B = 0.5$ (which provided the data for the least squares analysis). In Figure 9 the estimated crack tip parameters ($Ka^{i\varepsilon}$) and $\Delta(Ka^{i\varepsilon})_T$ are plotted as a function of temperature near the crack tip. The last data point corresponds to crack initiation. The temperature-induced deformations affect the imaginary part of the stress intensity factors as one would expect from the fringe patterns. The real part of the complex SIF is seen to undergo only a small increase.

Interfacial Crack Initiation

To investigate the failure mechanism associated with adhesively bonded bimaterial systems subjected to thermomechanical loading, several crack initiation experiments with three different initial loads were carried out. Here the role of thermal field on crack initiation when the initial applied load is a small fraction of the load that produces initiation under mechanical loading alone is examined. Results from these experiments with different initial loads (at $t = 0$ sec) are listed in Table 1 and are average values of three to four experiments for each case. It is important to note that upon heating, crack initiation occurs even when the load P is only a small fraction of the P_{cr-m} value. The results suggest an important difference when compared to the previously reported interfacial crack initiation results [8, 18]
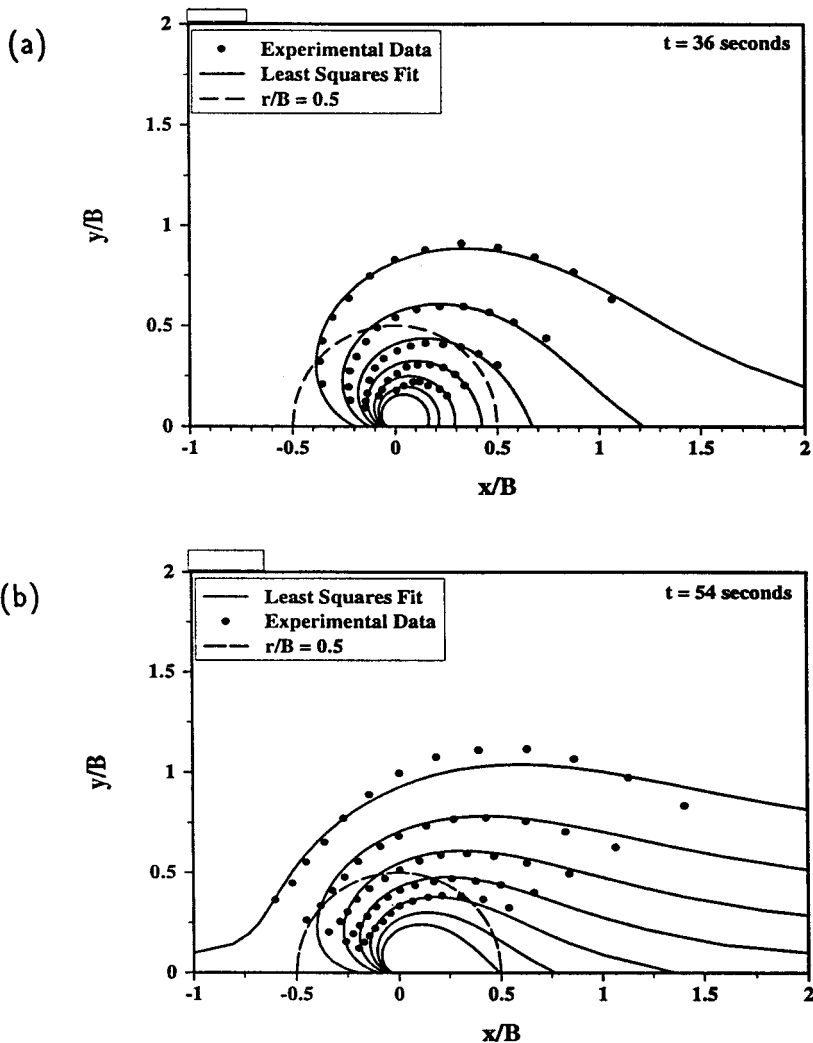
(a)

(b)

Figure 8. Least squares data analysis of thermal-mechanical fringes: (*a*) $t = 36$ sec and (*b*) $t = 54$ sec. Data within the semicircle ($r/B = 0.5$) are not used in the analysis.

under purely mechanical loading conditions that crack initiation toughness increases with increasing mode-mixity. This difference is potentially due to the crack initiation mechanism under thermomechanical loading conditions being different from that for purely mechanical loading conditions. To bring out this difference, the data from these tests are presented differently in Table 2. In each experiment, the crack initiation was seen to occur at approximately 70 sec (e.g., $t = 72$ sec in Table 1). The corresponding incremental increases $\Delta[\mathrm{Im}(Ka^{i\varepsilon})_{\mathrm{T}}]$ are relatively constant for all the three cases and are substantially higher than $\Delta[\mathrm{Re}(Ka^{i\varepsilon})_{\mathrm{T}}]$
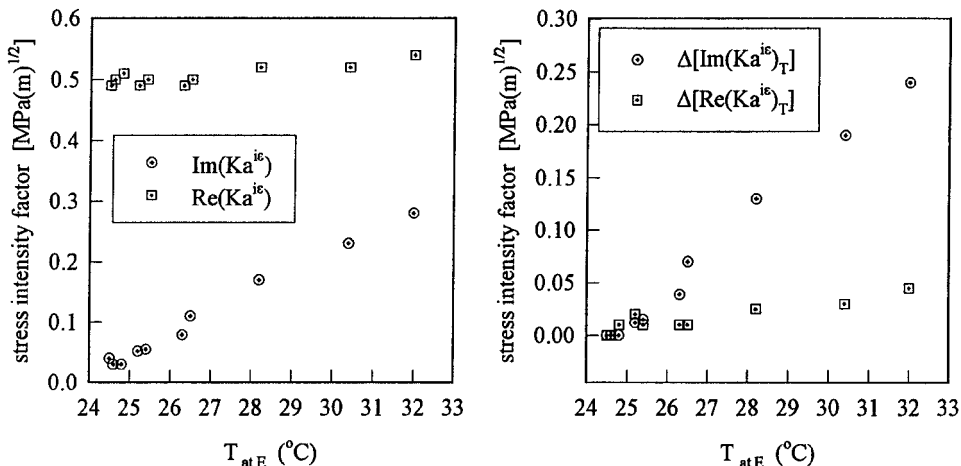
Figure 9. Variation of stress intensity factors with temperature ($P/P_{\mathrm{cr-m}} \approx 0.25$): (*a*) total values and (*b*) temperature-induced values.

values. Therefore, it can be concluded that transient heating primarily contributes to Im($Ka^{i\varepsilon}$) and, hence, the increased crack tip shear deformations. This increase, however, does not enhance the critical values of $|(Ka^{i\varepsilon})|$ in thermomechanical experiments unlike the mechanical counterparts [18]. *Thus, a strong dependence of crack initiation event on a micromechanical process controlled by the temperature-induced mismatch can be suspected.* In adhesive joints such as the one in question, the interfacial strength is primarily derived from micromechanical interlocking [23] and other adhesion mechanisms such as adsorption, chemical bonds, diffusion are

Table 1 Overall crack tip parameters at initiation [(SIFs in MPa$\sqrt{\mathrm{m}}$); $P_{\mathrm{cr-m}} = 925\,N \Rightarrow |Ka^{i\epsilon}|_{\mathrm{cr}} \approx 2.1\,\mathrm{MPa}\sqrt{\mathrm{m}}$, $\psi(a) \approx 10°$]

$(P/P_{\mathrm{cr-m}})$	$(P_{\mathrm{cr}}/P_{\mathrm{cr-m}})$	Re($Ka^{i\varepsilon}$)$_{\mathrm{cr}}$	Im($Ka^{i\varepsilon}$)$_{\mathrm{cr}}$	$\psi(a)$
0.12	0.18	0.28	0.25	42°
0.25	0.30	0.54	0.28	27°
0.50	0.54	1.04	0.29	16°

Table 2 Temperature-induced crack parameters at initiation ($P_{\mathrm{cr-m}} = 925\,N$; $|Ka^{i\epsilon}|_{\mathrm{cr}} \approx 2.1\,\mathrm{MPa}\sqrt{\mathrm{m}}$, $\psi \approx 10°$)

$(P/P_{\mathrm{cr-m}})$	$(P_{\mathrm{cr}}/P_{\mathrm{cr-m}})$	$\Delta[\mathrm{Re}(Ka^{i\varepsilon})_{\mathrm{T}}]$	$\Delta[\mathrm{Im}(Ka^{i\varepsilon})_{\mathrm{T}}]$	$\Delta\psi_{\mathrm{T}}(a)$
0.12	0.18	0.03	0.23	82°
0.25	0.30	0.04	0.24	81°
0.50	0.54	0.06	0.21	75°

rather weak. In the present situation, it is plausible that as the temperature in the aluminum half of the bimaterial system increases, the microcavities (due to sandblasting of aluminum) along the interface expand, resulting in a loss of interlocking between aluminum and PMMA. Because the thermal conductivity of PMMA is approximately one order lower than aluminum (although α_1 is about three times that of α_2), at a microscopic level aluminum cavities expand as the temperature rises and thereby disengage from the polymeric protrusions, causing a loss of mechanical interlocking. The presence of tensile stresses near the crack tip (due to the initial load) promote the unzipping process by breaking the weak adhesive bonds, if any, and help the crack to spread. This is supported by the fact that even a small initial applied load, as small as $P/P_{cr-m} \approx 0.12$, resulted in crack initiation. (Smaller initial loads also produced crack initiation but were optically difficult to resolve in the present experimental setup. However, the crack initiation was not optically detected in bonded but *unconstrained bimaterial specimens* even after 180 sec of heating.) The preceding failure mechanism is different from the one that occurs under purely mechanical loading situations where micromechanical interlocking between microcavities and microprotrusions, and the adhesive bonds have to be broken for the crack to spread.

   To conform this, crack tip regions in mechanically fractured and thermomechanically fractured specimens were examined. The fractured surfaces did not show any significant visible differences when examined macroscpically, and crack propagation was seen to occur along the adhesive and aluminum interface. However, a microscopic examination of the crack tip region revealed differences. Figures 10(a, b) show the micrographs of thermomechanically failed and mechanically failed aluminum halves of the crack tip region, respectively. Figure 10(a) shows a region close to the initial crack tip, and the surface texture essentially represents a typical sandblast surface. Further, no evidence of PMMA can be found on the fractured surface, implying a clean separation of the two materials and a crack initiation mechanism alluded to earlier for thermomechanically loaded specimens. On the contrary, the mechanical counterpart from Figure 10(b) shows a difference: there is evidence of PMMA in the aluminum pits, suggesting a failure event involving breakage of PMMA microprotrusions locked into the microcavities on the sandblasted aluminum face. Such a crack initiation event would obviously require relatively large crack-driving force quantified earlier.

   The crack initiation in thermomechanical experiments is seen to be rather independent of the initial load P. Hence, $\Delta(Ka^{i\varepsilon})_{T}(\Delta\psi_{T})$ was viewed as a potential crack initiation parameter in these cases. The corresponding value of the crack-driving force at initiation was $(G_{cr})_{T} \approx 10$ J/m^2. This value is substantially smaller than those reported for this bimaterial system under mechanical loading conditions (over a wide range of mode-mixities) by about one order of magnitude [8, 18]. It should be recognized that this investigation does not account for any loss of PMMA stiffness due to temperature rise. Approximately a 20% tensile modulus reduction for a temperature rise from 24°C to 70°C is reported[1] for acrylics. A first-order correction to account for this reduction would still produce a signifi-

---

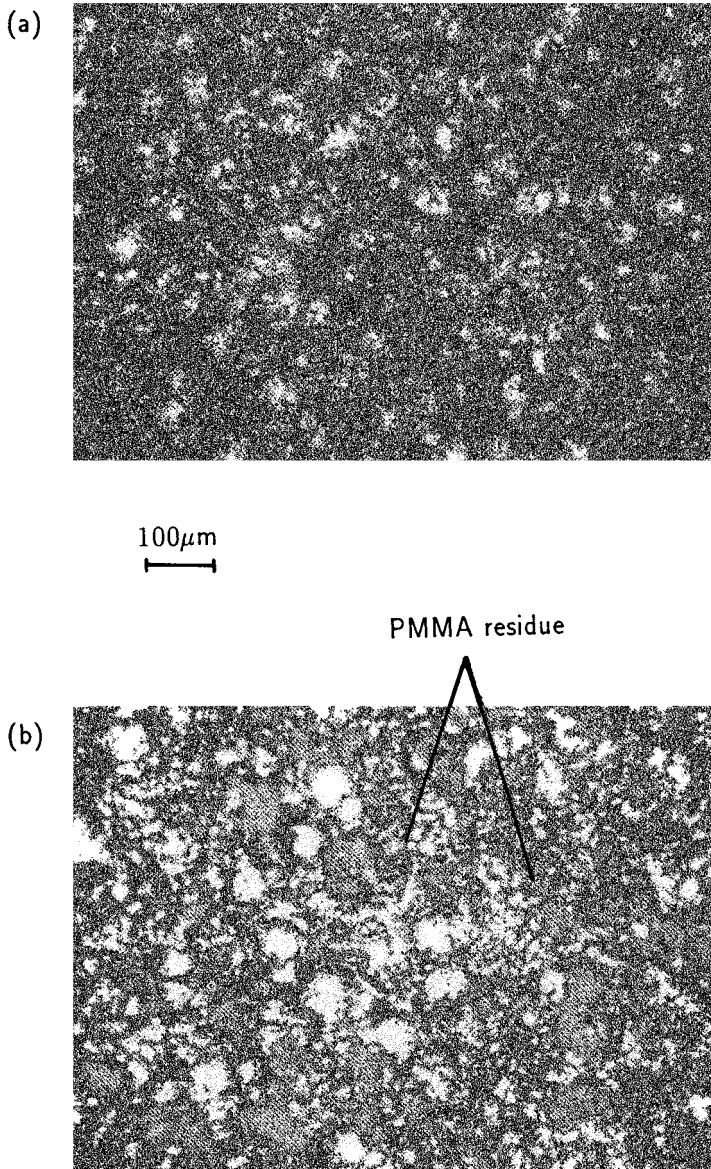[1] Swedlow, Inc., Garden Grove, CA.

(a)

100μm

PMMA residue

(b)

Figure 10. Micrographs of the fractured interface, aluminum half: (*a*) thermal-mechanical loading and (*b*) mechanical loading.

cantly lower value of crack initiation toughness compared to the mechanical counterparts.

CONCLUSIONS

An optical investigation dealing with the assessment of fracture parameters and the crack initiation mechanism in adhesively bonded bimaterial systems was carried out. Bimaterial joints with large elastic and thermal properties mismatch, which derive interfacial strength through micromechanical interlocking were examined. Under mechanical loading conditions interfacial fracture parameters were extracted from the optical interference measurements. The interface crack tip was then studied when subjected to thermally induced stresses by heating the metallic part of a constrained bimaterial beam. The thermal property mismatch stresses and hence the shear component of the complex stress intensity factor were affected by the temperature rise. The interference patterns from thermal-mechanical loading experiments were analyzed using interface crack tip fields and experimentally determined higher order terms for estimating fracture parameters.

The critical values of the stress intensity factors and the corresponding mode-mixities suggest that the crack initiation mechanism under thermomechanical conditions is different from the mechanical counterparts. The incremental values of $\Delta \mathrm{Im}(Ka^{i\varepsilon})_{\mathrm{T}}$ $(\approx \Delta(Ka^{i\varepsilon})_{\mathrm{T}}$ due to a temperature rise is constant for all the thermomechanical experiments and potentially a failure characterization parameter under thermomechanical loading conditions. Micrographs of the fractured surfaces were used to explain the differences. Under thermomechanical situations, a relative expansion between the microcavities and microprotrusions leads to a loss of micromechanical interlocking, which in turn increases the susceptibility of the crack for spreading. This is unlike the purely mechanical loading situations where fracture toughness is derived from the breakage of the microentanglements. The presence of crack tip tensile stresses due to the imposed constraint assist in the crack initiation event.

REFERENCES

1. M. L. Williams, The Stress Around a Fault or a Crack in Dissimilar Media, *Bull. Seismological Soc. Amer.*, vol. 49, no. 2, pp. 199–203, 1959.
2. J. R. Rice and G. C. Sih, Plane Problems of Cracks in Dissimilar Media, *J. Appl. Mech.*, vol. 32, pp. 418–423, 1965.
3. F. Erdogan, Stress Distribution in Bonded Dissimilar Materials with Cracks, *J. Appl. Mech.*, vol. 32, pp. 403–410, 1965.
4. H. C. Cao and A. G. Evans, An Experimental Study of the Fracture Resistance of Bimaterial Interfaces, *Mech. Materials*, pp. 295–301, 1989.
5. H. V. Tippur and A. J. Rosakis, Quasi-static and Dynamic Crack Growth along Bimaterial Interfaces: A Note on Crack Tip Field Measurements Using Coherent Gradient Sensing, *Exp. Mech.*, vol. 31, no. 3, pp. 243–252, 1991.
6. N. P. O'Dowd, C. F. Shih, and M. G. Stout, Test Geometries for Measuring Interfacial Fracture Toughness, *Int. J. Solids and Structures*, vol. 29, no. 5, pp. 571–589, 1992.

7. J. S. Wang and Z. Suo, Experimental Determination of Interfacial Toughness Curves Using Brazil-nut-sandwiches, *Acta Met.*, vol. 38, no. 7, pp. 2179–1290, 1990.

8. L. Xu and H. V. Tippur, Fracture Parameters for Interfacial Cracks: Optical Measurements and Finite Element Analysis, *Int. J. Fract.*, vol. 71, pp. 345–363, 1995.

9. J. K. Sinha, H. V. Tippur, and L. Xu, An Interferometric and Finite Element Investigation of Interfacial Crack Tip Stress Fields: Role of Mode-mixity on Stress Variations, *Int. J. Solids and Structures*, vol. 34, pp. 741–754, 1997.

10. J. W. Hutchinson and Z. Suo, Mixed Mode Cracking in Layered Materials, *Adv. Appl. Mech.*, vol. 29, pp. 63–191, 1992.

11. J. R. Rice, Elastic Fracture Mechanics Concepts for Interfacial Cracks, *J. Appl. Mech.*, vol. 55, pp. 98–103, 1988.

12. E. J. Brown and F. Erdogan, *Int. J. Eng. Sci.*, vol. 6, pp. 517–529, 1968.

13. A. Y. Kuo, Interface Crack Between Two Dissimilar Half Spaces Subjected to a Uniform Heat Flow at Infinity-Open Crack, *J. Appl. Mech.*, vol. 57, pp. 359–364, 1990.

14. K. J. Kokini, Interfacial Cracks in Ceramic-to-Metal Bonds under Transient Thermal Loads, *J. Amer. Ceramic Soc.*, vol. 70, pp. 855–859, 1987.

15. K. Kokini and C. C. Smith, Interfacial Transient Thermal Fracture of Adhesively Bonded Dissimilar Materials, *Exp. Mech.*, vol. 29, no. 3, pp. 312–317, 1989.

16. K. P. Herrmann, A. Noe, and M. Dong, Interfacial Crack Growth in Thermo-mechanically Loaded Bimaterial Joints, *Composites*, Pt. A, Vol. 27A, pp. 813–820, 1996.

17. S. Ramaswamy, H. V. Tippur, and L. Xu, Mixed-mode Crack Tip Deformations Studied Using a Modified Flexural Specimen and Coherent Gradient Sensing, *Exp. Mech.*, vol. 33, no. 3, pp. 218–227, 1993.

18. H. V. Tippur and L. Xu, Interfacial Crack Initiation under Quasi-static and Dynamic Loading Conditions: An Experimental Study, *Fatigue and Fract. Eng. Materials and Structures*, vol. 20, no. 1, pp. 49–60, 1997.

19. N. P. Dowling, *Mechanical Behavior of Materials*, Prentice-Hall, Englewood Cliffs, NJ, 1995.

20. R. Mahajan and A. S. Voloshin, Transient Stress Intensity Factors for Thermally Loaded Edge Cracked Plates, *J. Thermal Stresses*, vol. 16, pp. 197–207, 1993.

21. G. C. Sih, On the Singular Character of Thermal Stresses Near a Crack Tip, *J. Appl. Mech.*, vol. 9, pp. 587–589, 1962.

22. H. Krishnamoorthy and H. V. Tippur, Extracting Practure Parameters using Local Collocation of Full-field Displacement Data: A Modified Approach, *Exp. Tech.*, Nov./Dec. 1997, to appear.

23. L. Lee, *Adhesive Bonding*, Plenum Press, NY, 1991.